Structure of (FexCa1-xO)y(SiO2)1-y liquids and glasses from high-energy x-ray diffraction: Implications for the structure of natural basaltic magmas

Structure of $(Fe_xCa_{1-x}O)_y(SiO_2)_{1-y}$ liquids and glasses from high-energy x-ray diffraction: Implications for the structure of natural basaltic magmas

James W. E. Drewitt,[1,*] Chrystele Sanloup,[1] Aleksei Bytchkov,[2,3] Séverine Brassamin,[4] and Louis Hennet[4]

[1]*Centre for Science at Extreme Conditions (CSEC), School of Physics and Astronomy, University of Edinburgh, Edinburgh, EH9 3JZ, United Kingdom*

[2]*Institut Laue Langevin (ILL), 6 rue Jules Horowitz, BP 156, 38042 Grenoble, France*

[3]*European Synchrotron Radiation Facility (ESRF), 6 rue Jules Horowitz, BP 220, 38043 Grenoble cedex 9, France*

[4]*Conditions Extrêmes et Matériaux : Haute Température et Irradiation (CEMHTI), CNRS, Université d'Orléans, 1d avenue de la Recherche Scientifique, 45071 Orléans cedex 2, France*

(Received 8 April 2013; revised manuscript received 15 May 2013; published 3 June 2013)

The atomistic structure of $(Fe_xCa_{1-x}O)_y(SiO_2)_{1-y}$ liquids, namely, fayalite ($x = 1$, $y = 0.667$), ferrosilite ($x = 1$, $y = 0.5$), and hedenbergite ($x = 0.5$, $y = 0.5$), was measured by using high-energy x-ray diffraction combined with laser-heated aerodynamic levitation. Measurements were also made for hedenbergite glass, formed via supercooling the liquid. The results unequivocally prove that Fe atoms are both four and sixfold coordinated by oxygen atoms in all compositions studied from the two distinct bond distances measured at $r_{FeO} = 1.93$ and 2.20 Å, respectively. The results quantitatively reveal up to 40% and 55% FeO_6 species residing in liquid fayalite and ferrosilite, respectively. From the real-space peak positions, the results also reveal the presence of both FeO_4 and FeO_6 species within a basaltic liquid and glass for which the geophysical consequences are briefly discussed.

DOI: 10.1103/PhysRevB.87.224201 PACS number(s): 61.20.−p, 61.05.cp

I. INTRODUCTION

Silicate minerals containing iron, magnesium, and calcium constitute a major fraction of the composition of the Earth's mantle. Iron is arguably the most important cation in natural magmatic liquids as it has a strong influence on physical properties such as density and viscosity.[1] The $(Fe_xCa_{1-x}O)_y(SiO_2)_{1-y}$ system is of particular geological interest because fayalite ($x = 1$, $y = 0.667$) represents the iron-rich end member of the olivine solid solution series, while ferrosilite ($x = 1$, $y = 0.5$) and hedenbergite ($x = 0.5$, $y = 0.5$) are important pyroxene end members. As well as their geophysical significance, the CaO-FeO-SiO_2 system is also of importance in metallurgical smelting processes.[2] Detailed knowledge of the atomistic liquid structure and the local coordination environment of cations in silicate melts and glasses is of fundamental importance for improving our understanding of, e.g., magma-related processes.

Iron occurs in both ferric (Fe^{3+}) and ferrous (Fe^{2+}) oxidation states, both of which usually exhibit sixfold coordination with oxygen in crystalline minerals. Under ambient conditions, crystalline fayalite belongs to the orthorhombic space group *Pbnm*.[3] The Fe ions occupy two symmetrically distinct octahedral sites, denoted M(1) and M(2), which share edges and form serrated chains cross linked by isolated SiO_4 tetrahedra. Ferrosilite (orthorhombic space group *Pbca*)[4] and hedenbergite (monoclinic space group $C12/c$)[5] are ferrous chain silicates in which SiO_4 tetrahedra are corner linked to form linear chains. In ferrosilite, serrated chains are formed from two distinct edge sharing Fe^{2+} sites, M(1) (regular octahedra) and M(2) (distorted octahedra). In hedenbergite, serrated chains of M(1) sites are sandwiched between two linear chains of M(2) sites in which Ca^{2+} ions form distorted eightfold coordinated polyhedra.

The Fe coordination environment is less certain in iron silicate liquids and glasses. Extensive studies have been made on both natural and synthetic glass compositions, which have often been interpreted as analogs of the melt structure.[6–41] Various distributions of four, five, and sixfold coordinated Fe sites are reported, the proportions of which appear to be dependent on both the silicate composition and iron redox state.[19,29,31] Ferric iron (Fe^{3+}) mainly occupies sites with tetrahedral geometry in silicate glasses, although higher coordination species are possible.[12,13,24,29,31,32,34] In general, ferrous iron (Fe^{2+}) tends to occupy a distribution of four, five, and sixfold coordination sites with oxygen, where interpretations of x-ray absorption spectroscopy (XAS) measurements suggest that four and fivefold coordinated Fe sites dominate.[22,23,25,30,34,36] This result is, however, in contrast to Raman and optical absorption spectra, which report Fe^{2+} in sixfold coordination.[6,7,9,17,18,42]

By comparison, very little direct information is available on the local coordination environment in iron silicate melts due to the difficulty of performing experiments at high temperatures. Information obtained from the glasses is of limited use as an analog to liquids, as studies have shown that the structure of glass forming liquids can change dramatically when quenched into the solid state.[1,43] It is therefore advantageous to characterize the liquid structure *in situ*. It is difficult to employ nuclear magnetic resonance (NMR) spectroscopy due to the very low sensitivity and natural abundance of the spin-1/2 ^{57}Fe nucleus. X-ray diffraction, on the other hand, is particularly sensitive to the iron environment due to the relatively high atomic number $Z(Fe) = 26$ giving rise to a large scattering power by comparison with lighter elements such as Si and O. Waseda *et al.*[44,45] were the first to measure the structure of iron silicate liquids using conventional *in situ* x-ray diffraction (XRD) and reported a reduction in the Fe coordination from six to fourfold with increasing SiO_2 concentration. Their results are, however, controversial as they contain several inaccuracies, including an unrealistically small Fe-Si bond distance. Using *in situ* x-ray absorption spectroscopy (XAS) techniques, Jackson *et al.*[46] and Waychunas *et al.*[47] reported a

complete conversion of Fe^{2+} from higher coordinated species (six or fivefold) to fourfold coordinated Fe^{2+} in liquid Fe_2SiO_4 and $M_2FeSi_3O_8$ (M = Li, Na, K, Ca), respectively. In a more recent XAS study on binary alkali-silicate and haplogranitic compositions, Wilke *et al.*[34] show that although the melts do contain a higher concentration of fourfold coordinated Fe^{2+} than their glassy counterparts, the observed change in speciation is much smaller than that reported from the previous studies,[46,47] i.e., there is not a complete conversion to fourfold coordinated iron in the melt. Keppler[17] found that in albite and albite-diopside melts, Fe^{2+} predominantly resides in distorted octahedrally coordinated sites.

Recent advances in containerless heating methods, specifically aerodynamic levitation with laser heating, eliminate undesirable contamination from containment material and enable us to make high quality *in situ* measurements of liquid oxides at ambient pressure with temperatures up to 3000 K.[43,48,49] In this paper, we present the results of high-energy synchrotron x-ray diffraction measurements of aerodynamically levitated and laser heated iron silicate liquids. A comparison is made with the liquid structure also measured for a naturally occurring basalt. A preliminary account of the present liquid fayalite measurements is given in Ref. 50.

II. THEORY

In a synchrotron x-ray diffraction experiment, the total structure factor $S(Q)$ measured for a liquid sample of n chemical species α or β is given by the weighted sum of $n(n+1)/2$ Faber-Ziman[51] partial structure factors $S_{\alpha\beta}(Q)$, as given by

$$S(Q) - 1 = \sum_{\alpha=1}^{n}\sum_{\beta=1}^{n} \frac{c_\alpha c_\beta f_\alpha(Q) f_\beta^*(Q)}{|\sum_\alpha c_\alpha f_\alpha(Q)|^2}[S_{\alpha\beta}(Q) - 1], \quad (1)$$

where Q is the scattering vector, c_α and c_β are the atomic concentration of the corresponding chemical species α or β, $f_\alpha(Q)$ and $f_\beta(Q)$ are complex valued x-ray form factors, the asterisk denotes the complex conjugate and $|x|^2$ is the norm of x squared. If we define the weighting factor

$$\mathcal{W}_{\alpha\beta}(Q) = \frac{c_\alpha c_\beta f_\alpha(Q) f_\beta^*(Q)}{\left|\sum_\alpha c_\alpha f_\alpha(Q)\right|^2}, \quad (2)$$

then the total pair distribution function $G(r)$, giving us the structural information in real space, is obtained by the Fourier transform relation

$$\begin{aligned} r[G(r) - 1] &= \frac{1}{2\pi^2 n_0}\int_0^\infty Q[S(Q) - 1]\sin(Qr)\mathrm{d}Q \\ &= \sum_{\alpha=1}^{n}\sum_{\beta=1}^{n} r[g_{\alpha\beta}(r) - 1] \otimes \widetilde{\mathcal{W}}_{\alpha\beta}(r), \end{aligned} \quad (3)$$

where n_0 denotes the atomic number density, r is a distance in real space, $\widetilde{\mathcal{W}}_{\alpha\beta}(r)$ is the real space Fourier transform of $\mathcal{W}_{\alpha\beta}(Q)$, and $\otimes$ is the one-dimensional convolution operator. In practice, measurements are made up to a finite maximum scattering vector $Q_{\max}$, which leads to a multiplication of the $S(Q)$ prior to transformation with a modification function $M(Q)$, which can introduce undesirable Fourier transform artifacts. In the simplest case, $M(Q)$ is defined by a rectangular function, where $M(Q < Q_{\max}) = 1$ and $M(Q_{\max}) = 0$. In this paper, we employ a window function with a cosine modulation applied within a specific Q range from Q_1 to Q_2, where

$$M(Q) = \begin{cases} 1 & \text{if} \quad Q < Q_1 \\ 0.5\left[1 + \cos\left(\frac{x\pi}{N-1}\right)\right] & \text{if} \quad Q_1 \leqslant Q \leqslant Q_2 \\ 0 & \text{if} \quad Q > Q_2. \end{cases} \quad (4)$$

Here, N is the width of the window function and x is an integer with values $0 \leqslant x \leqslant N-1$.

Difficulties arise when interpreting the measured $G(r)$ function in terms of its constituent partial pair distribution functions $g_{\alpha\beta}(r)$ due to their convolution with r-dependent weighting factors, arising from the Q dependency in the atomic form factors, which tends to broaden the peaks in $G(r)$. Inaccuracies can therefore arise in the calculation of coordination numbers from the area under a peak at position r arising from a specific $g_{\alpha\beta}(r)$ function, as given by

$$\bar{n}_\alpha^\beta = 4\pi n_0 c_\beta \int_{r_i}^{r_j} g_{\alpha\beta}(r) r^2\,\mathrm{d}r, \quad (5)$$

where $\bar{n}_\alpha^\beta$ is the mean coordination number of atoms of type β contained in spherical coordination shell of radius $r_i < r < r_j$ in which an atom α is at the center. Several methods can be employed to obtain reliable approximations for the coordination number in x-ray diffraction data. If there is a clearly defined peak in $G(r)$ that can be assigned to a particular $g_{\alpha\beta}(r)$ function, then it is convenient to divide the $S(Q)$ function by the weighting factor applied to $S_{\alpha\beta}(Q)$ prior to transformation, such that the r-dependent weighting factor on the $g_{\alpha\beta}(r)$ function of interest is removed in the Fourier transform.[52] Alternatively, where several correlations clearly overlap, a model may be obtained by fitting a suitable number of Gaussian functions to the real-space peaks. A constant value for the form factors may then be used by taking, e.g., an average value over all Q space[53] or by simply taking the value at $Q = 0$.

III. SAMPLE PREPARATION

The basalt (β-PST9) sample had a composition, relative to eight oxygens, of $Na_{0.216}Mg_{0.57}Ca_{0.645}K_{0.115}Mn_{0.007}Ti_{0.03}P_{0.026}Al_{0.869}Fe_{0.317}Si_{2.436}O_8$. This corresponds to the composition of natural golden pumice samples found at the present day Stromboli volcano (Aeolian Islands, Italy).[54,55] Naturally occurring fayalite, Fe_2SiO_4 (Alfa Aesar, 0.06–0.19 in. grains), was used as supplied by the manufacturer. The ferrosilite and hedenbergite samples were synthesized by mixing powdered fayalite in an agate mortar with crystalline silicon (IV) oxide, SiO_2 (Aldrich, $\geqslant$99.9%), and calcium silicate, $CaSiO_3$, (Aldrich, $\geqslant$99%) powders, weighed in the correct stoichiometric proportions. A small ($\sim$1 mol.%) excess of SiO_2 was added to the ferrosilite composition to limit the formation of fayalite.[56] The powders were packed into Fe capsules of length 13(1) mm, outer diameter 2.30 mm, and wall thickness 0.115 mm. The capsules were crimped at both ends and pressurized to 1.5(1) GPa at 1073(2) K for 26–28 hours in a Piston-cylinder press (Quick Press, Depths of the Earth Company). The resulting materials gave Raman spectra consistent with the required compositions. The materials were levitated in air on an argon gas flow and partially

premelted by laser heating in order to form solid spherical samples of 3.0(2) mm diameter.

IV. EXPERIMENTAL METHOD

High-energy x-ray diffraction measurements were made on the high-temperature liquids using an aerodynamic levitation and laser heating device installed at the ID15 beamline at the European Synchrotron Radiation Facility (ESRF) with an incident x-ray wavelength of $\lambda_0 = 0.12454$ Å, corresponding to an energy of 99.554 keV, and a beam size of 250 μm horizontally and 50 μm vertically. The experimental setup was a modified setup originally constructed for the ID11 beamline reported in Ref. 57. The samples were levitated by an argon gas flow through an aluminium nozzle and heated above their melting points using two 125-W CO_2 laser beams. The ferrosilite sample was melted in a pure Ar atmosphere, while all other samples were heated under normal atmospheric conditions. Up to 120 individual two-dimensional diffraction patterns, with acquisition times of 100 or 500 ms, depending on the limit of detector saturation, were measured for each sample using a Perkin-Elmer detector providing a wide Q range extending to 26.45 $Å^{-1}$. The samples were rapidly cooled by cutting the laser power. This resulted in the formation of opaque glasses for the hedenbergite and basalt melts for which diffraction patterns were also measured under ambient atmospheric conditions. Additional measurements were also made for the background scattering intensity from the empty aluminium levitation nozzle in air and argon, and for a silicon calibrant.

The individual diffraction patterns were corrected for geometrical effects and incident beam polarization and reduced to one-dimensional patterns using the program FIT2D[58,59] and normalized to the incident beam intensity. For each sample, the measured diffraction intensities were averaged and corrected for dark current noise and background scattering before being scaled to fit the sum of the Compton and self-scattering contributions at $Q \gtrsim 4.5$ $Å^{-1}$, where the Compton scattering cross sections were taken from the tables reported by Hubbell *et al.*[60] and the atomic form factors are reported in the international tables of x-ray crystallography.[61] Some additional spikes arising from electronic noise of the detector that were not sufficiently removed by the dark current subtraction were eliminated by applying a median filter to the data sets. The elements in the measured sample compositions all have very small absorption coefficients for the incident x-ray energy employed. As such, the imaginary part of the x-ray form factors are negligible and have been ignored. The self and Compton scattering contributions were subtracted to obtain the Rayleigh-Thomson differential scattering cross-section from which the total structure factor $S(Q)$ defined in Eq. (1) was obtained.

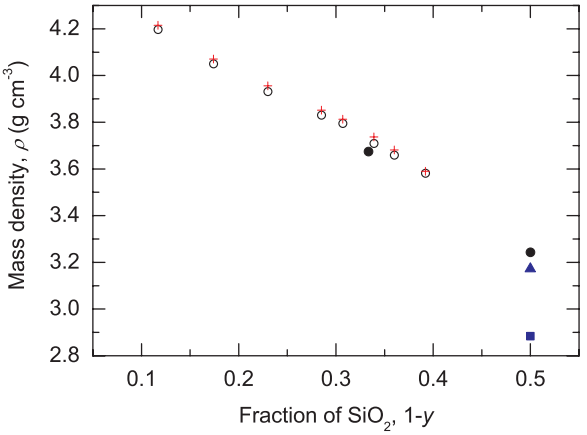

FIG. 1. (Color online) Mass density of the measured iron silicates. The red crosses and the open black circles are the results from Shiraishi *et al.*[62] for $(FeO)_y(SiO_2)_{1-y}$ liquids at 1300 and 1400 °C, respectively. The solid black circles are the densities used for liquid fayalite and ferrosilite in the present measurements. The solid blue square and triangle are the densities used for liquid and glassy hedenbergite, respectively.

The measured data sets were checked for self-consistency by ensuring that (i) each $S(Q)$ obeys the sum-rule relation $\int_0^\infty [S(Q) - 1]Q^2 dQ = -2\pi n_0$, which follows from the $r = 0$ limit of Eq. (3), (ii) the unphysical low-r features in each $G(r)$ oscillate about the theoretical $G(r = 0) = 0$ limit, and (iii) the Fourier back transform of the $G(r)$ functions, with the low-r features up to the onset of the first physical peak set to the $G(r = 0) = 0$ limit, are in good overall agreement with the measured $S(Q)$ functions.[52] The density for the liquids and glasses were obtained by using the values that best satisfied steps (i)–(iii) above. For the $(Fe_xCa_{1-x}O)_y(SiO_2)_{1-y}$ compositions, the values are shown in Fig. 1 by comparison with the density measurements reported by Shiraishi *et al.*[62] The densities for the basalt liquid and glass are listed in Table I.

Following the diffraction measurements, the recovered samples were embedded in epoxy, polished, and C coated.

TABLE I. First peak or shoulder positions in reciprocal space q_1, q_2 and real space r_{SiO}, r_2, r_3, r_4 together with the coordination numbers $\bar{n}^O_{Si}$, $\bar{n}^O_{Fe}$ for the $(Fe_xCa_{1-x}O)_y(SiO_2)_{1-y}$ or basalt (β-PST9) samples at temperature T measured at the ID15 beamline. The mass density ρ and corresponding number densities n_0 are also given.

Sample						$S(Q)$		$G(r)$					
	x	y	T(K)	ρ(gcm^{-3})	n_0(Å^{-3})	q_1(Å^{-1})	q_2(Å^{-1})	r_{SiO}(Å)	r_2(Å)	r_3(Å)	r_4(Å)	$\bar{n}^O_{Si}$	$\bar{n}^O_{Fe}$
Fayalite	1	0.667	1623(30)	3.67(4)	0.076(1)	2.15(2)	4.14(3)	1.64(1)	1.93(1)	2.20(2)	2.54(3)	4.0(1)	4.8(2)
Ferrosilite	1	0.5	1683(30)	3.24(4)	0.074(1)	2.10(2)	4.23(3)	1.66(1)	1.93(1)	2.20(2)	2.55(3)	4.0(1)	5.1(2)
Hedenbergite	0.5	0.5	1623(30)	2.88(4)	0.070(1)	1.93(2)	4.21(3)	1.64(1)	1.93(1)	2.24(2)	2.55(3)	4.0(1)	–
Hedenbergite	0.5	0.5	300(1)	3.17(4)	0.077(1)	1.97(2)	4.15(3)	1.64(1)	1.96(1)	2.27(2)	2.55(3)	4.0(1)	–
Basalt (β-PST9)			1623(30)	2.91(4)	0.080(1)	1.83(2)	4.38(3)	1.66(1)	1.92(1)	2.25(2)	2.72(3)	4.0(1)	–
Basalt (β-PST9)			300(1)	3.27(4)	0.090(1)	1.81(2)	4.34(3)	1.65(1)	1.96(1)	2.30(2)	2.69(3)	4.0(1)	–

Chemical analysis of the quenched samples was performed using a Cameca SX100 electron probe microanalyzer (EMMAC, University of Edinburgh) operating with 15 kV accelerating voltage and a focused beam for point analysis. Back scattered electron images revealed complete homogeneity in each sample. Analyses of well-characterized standards of synthetic fayalite and a basaltic glass composition (BCR2g[63]) were made for calibration purposes. The quenched samples retained a stoichiometry close to their starting compositions, where the mean analyses reveal the final compositions to be $Fe_{1.82}Si_{1.03}O_4$ (fayalite), $Fe_{1.04}Si_{0.95}O_3$ (ferrosilite), $Fe_{0.49}Ca_{0.48}Si_{0.98}O_3$ (hedenbergite), and $Na_{0.203}Mg_{0.57}Ca_{0.656}K_{0.102}Mn_{0.006}Ti_{0.029}P_{0.008}Al_{0.89}Fe_{0.307}Si_{2.447}O_8$ (β-PST9). Trace quantities of Ca, Mg, and Mn were also detected in the ferrosilicate samples. The analysis of the ferrosilite sample yielded a deficient oxide sum indicating the presence of an appreciable concentration of Fe^{3+} ions.

V. RESULTS

The measured total structure factors $S(Q)$ are shown in Fig. 2. The $S(Q)$ functions were Fourier transformed after applying a cosine window function to the data sets between $21.45 \leqslant Q(\text{Å}^{-1}) \leqslant 26.45$ [see Eq. (4)] and the resulting total pair distribution functions $G(r)$ are shown in Fig. 3. The first few peak positions in both reciprocal and real space are given in Table I, together with the mass and number densities of the samples at the experimental temperatures. The first peak in the $G(r)$ functions at 1.64(1)–1.66(1) Å in all the compositions measured is attributed to the nearest-neighbor Si-O correlations, by comparison with the first Si-O distance in the corresponding crystalline structures,[3–5] while the next two peaks in r space are attributed to Fe-O correlations (as discussed below). The first few peaks in the total correlation function $T(r) = 4\pi r n_0 G(r)$ for liquid fayalite and ferrosilite were fitted using a superposition of Gaussian functions, as shown in Fig. 4. The coordination numbers, $\bar{n}^{\text{O}}_{\text{Si}}$ and $\bar{n}^{\text{O}}_{\text{Fe}}$, as obtained by integrating over the area of the fitted Gaussian functions according to Eq. (5), are given in Table I. The error in the coordination numbers arises in part to the fact that the Gaussian fitting procedure does not take into account any asymmetry in the underlying correlations that contribute to the fitted real space peaks nor the broadening effect in real space of the modification function $M(Q)$ [see Eq. (4)].

While it was possible to fit a Gaussian function to the Si-O peak in the hedenbergite $T(r)$ functions, the large degree of ambiguity arising from the partial pair distribution functions in both the hedenbergite and basaltic compositions precluded the use of a full Gaussian model for these samples. The relatively invariant nature of the Si-O peak position enabled the reasonable assumption of that the coordination number $\bar{n}^{\text{O}}_{\text{Si}} = 4.0(1)$ obtained in the fayalite, ferrosilite, and hedenbergite samples remains constant in the more complex basaltic composition.

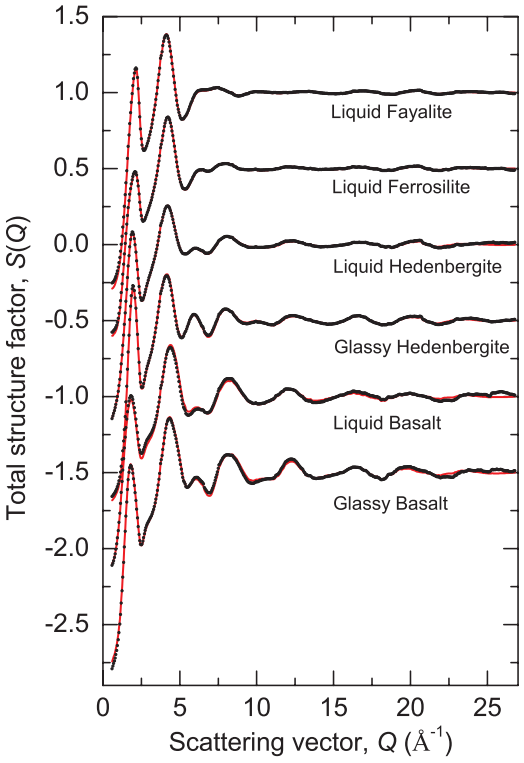

FIG. 2. (Color online) The total structure factors $S(Q)$ for the iron silicate and basaltic liquids and glasses measured on beamline ID15 at the ESRF (closed black circles). The solid red curves are the Fourier back-transforms of the corresponding real space functions shown in Fig. 3, after the low-r features up to the first interatomic distance are set to the $r = 0$ limit. The results are displaced vertically for clarity of presentation.

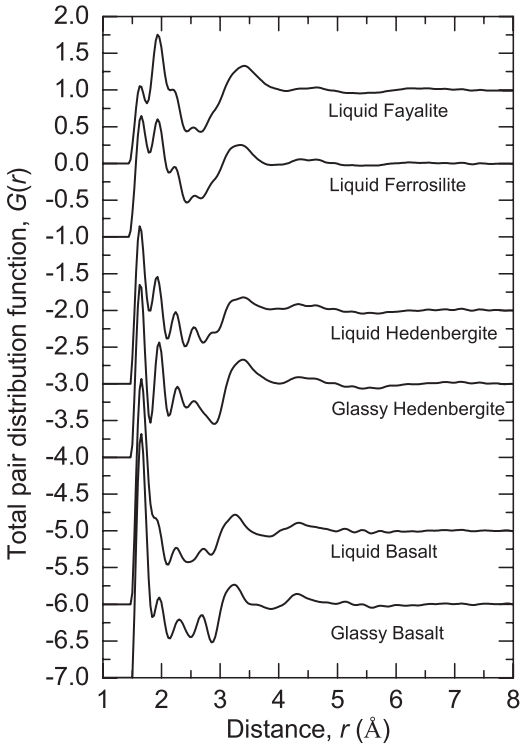

FIG. 3. The total pair distribution functions $G(r)$ for the iron silicate and basaltic liquids and glasses as obtained by Fourier transforming the corresponding $S(Q)$ functions shown in Fig. 2. For clarity of presentation, the small-r oscillations below the onset of the first physical peak are omitted, and the results are displaced vertically.

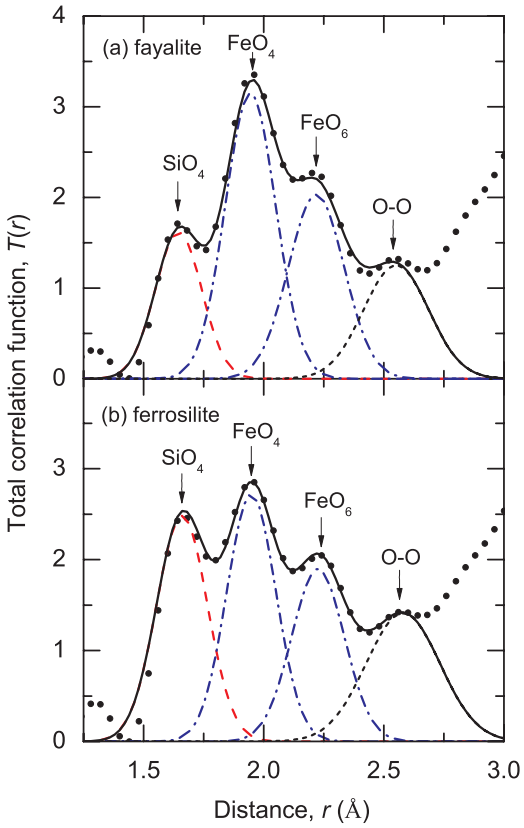

FIG. 4. (Color online) Gaussian fits to main peaks in the measured $T(r)$ functions for (a) liquid fayalite, and (b) liquid ferrosilite. The solid (black) circles represent the measured data, the long dashed (red) curves are the fits to the Si-O nearest neighbor peak, the chained (blue) curves are the fits to the first and second Fe-O peaks, the short dashed (black) curves approximate contributions arising from O-O correlations, and the solid black curves are the superposition of all the fitted Gaussians. The arrows indicate the positions of the Si-O, Fe-O, and O-O peaks.

The local coordination environment for iron in silicate melts and glasses is complicated by its multivalent character, whereby Fe^{3+} and Fe^{2+} ions preferentially occupy different coordination sites. Fe ions in both oxidation states can occupy a distribution of coordination sites in which typical Fe-O bond lengths for model crystalline silicate compounds are 1.98 and 1.86 Å for fourfold Fe^{2+} and Fe^{3+}, respectively, to 2.12 and 2.02 Å for sixfold coordinated Fe^{2+} and Fe^{3+} species, respectively.[19] The peak observed at $r_2 = 1.93(1)$ Å and shoulder at $r_3 = 2.20(2)$ Å in the $G(r)$ for liquid fayalite are therefore representative of two distinct Fe^{2+} coordination sites, corresponding to fourfold coordinated FeO_4 tetrahedra and sixfold coordinated FeO_6 octahedra, respectively. Although it is not possible to directly determine the oxidation speciation in these sites by using diffraction methods, the bond distances are consistent with a predominance of Fe^{2+} speciation, in concurrence with the electron probe microanalysis measurements. The peak at 2.54(3) Å is attributed to O-O correlations, by comparison with the smallest distance $r_{OO} = 2.550$ Å present in the crystalline structure.[3] Integrating over the sum of the areas of the Gaussian functions fitted to the FeO_4 and FeO_6 peaks [see Fig. 4(a)] yields an average coordination number $\bar{n}^{O}_{Fe} = 4.8(2)$.

Similarly, we find the same two Fe-O bond lengths in the $G(r)$ for liquid ferrosilite associated with FeO_4 and FeO_6 species. The peak at $r_4 = 2.55(3)$ Å is comparable to the smallest bond length $r_{OO} = 2.514$ Å found in crystalline ferrosilite.[4] An average coordination number of $\bar{n}^{O}_{Fe} = 5.1(2)$ is found by integrating over the sum of the area of the Gaussian functions fitted to the peaks associated with FeO_4 and FeO_6 species in $T(r)$ [see Fig. 4(b)].

The addition of Ca in the hedenbergite composition increases the level of ambiguity in the interpretation of features in real space via the introduction of additional atomic pair correlations, e.g., Ca-O. As for the fayalite and ferrosilite liquids, the peak observed at $r_2 = 1.93(1)$ Å for liquid hedenbergite can be attributed to FeO_4 polyhedra. In a recent neutron diffraction with isotope substitution and molecular dynamics (MD) computer simulation study of liquid and glassy $CaSiO_3$,[64] the Ca-O bond length was measured as 2.35 Å. This compares well with the smallest bond distance $r_{CaO} = 2.348$ Å found in crystalline hedenbergite[5] and gives rise to Ca-O correlations that overlap the sixfold coordinated Fe-O peak position, resulting in the observed shift to a slightly higher position $r_3 = 2.24(2)$ Å compared to the fayalite and ferrosilite liquids. The peak at $r_4 = 2.55(3)$ Å is attributed to O-O correlations by comparison with the O-O distance reported for liquid and glassy $CaSiO_3$,[64] and is close to the smallest bond length $r_{OO} = 2.649$ Å present in the crystal structure.[5] For the hedenbergite glass, both the four- and sixfold coordination peaks are shifted to slightly higher values of $r_2 = 1.96(1)$ Å and $r_3 = 2.27(1)$ Å, respectively, compared to the liquid counterparts.

By comparison with the previous iron silicate samples, the measured basalt has a very complicated composition and the results contain many more overlapping correlations. The first peak measured at 1.66(1) Å can be attributed to the nearest-neighbor Si-O correlations. It is, however, overlapped by other correlations (e.g., Al-O, Mg-O). Despite this added complexity, the results for the Fe-Ca-Si-O compositions can provide us with insight into the local structure. Even though Fe has a relatively low atomic fraction (2.4%) in the basalt composition, it is strongly probed by x rays and as such the Fe-O correlations are relatively well resolved by comparison to the correlations of lighter elements. The two peaks observed at 1.92(1) and 2.25(2) Å in liquid basalt, and the corresponding peaks at 1.96(1) and 2.30(2) Å in the glass, are therefore indicative of the presence of two distinct sites associated with FeO_4 and FeO_6 polyhedra, as observed in the simpler Fe-Ca-Si-O compositions.

VI. DISCUSSION

A. Comparison of the liquid fayalite measurements with a previous conventional x-ray diffraction study

The only previous diffraction measurements reported for molten iron silicates were made by Waseda *et al.*[44,45] The authors used a conventional x-ray diffraction technique, for which there are a number of limitations by comparison with synchrotron x-ray diffraction, including strong absorption,

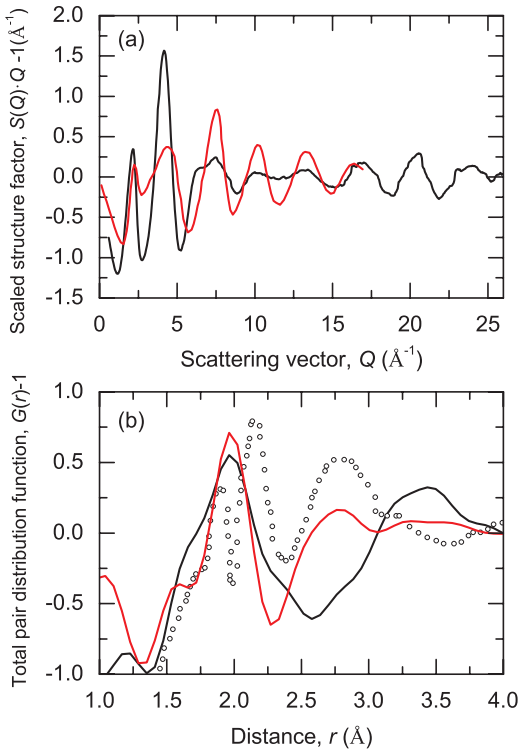

FIG. 5. (Color online) (a) The scaled total structure factor $S(Q)Q$ for liquid fayalite at $T = 1623$ K, as measured by Waseda *et al.*[44] (light (red) curve) by using conventional x-ray diffraction methods, as compared with the present synchrotron x-ray diffraction measurement (dark (black) curve). (b) The total pair distribution functions for liquid fayalite up to 4.0 Å as obtained by Fourier transformation of the corresponding $S(Q)Q$ functions of Waseda *et al.*[44] [light (red) curve] and the present measurements [dark (black) curve] given in (a). The open (black) circles show the original data digitized from Ref. 44.

which leads to limited bulk structure penetration. A number of inconsistencies are found between the previous study and the present measurements, as described below. In Fig. 5, we show the $S(Q)$ function, scaled by Q, and corresponding $G(r)$ function for fayalite at $T = 1623$ K reported in Ref. 44. For comparison, we also show the Q-scaled $S(Q)$ for fayalite from the present measurements and the associated $G(r)$ function obtained by truncating at the same $Q_{\max} = 16.94$ Å^{-1}. In reciprocal space, the measurements by Waseda *et al.*[44] show features resolved with a similar periodicity as for our measurements, however, the amplitudes and subtle structural features are not resolved. In real space, there is no well defined peak at 1.62 Å, which the authors attributed to the nearest neighbor Si-O distance. The authors also assigned the Fe-Si correlations an unphysical interatomic distance of 1.81 Å from the position of their second peak in real space. This value is much lower than the minimum distance $r_{\mathrm{FeSi}} = 2.785$ Å found in crystalline fayalite.[3]

To investigate these inconsistencies, we made a Fourier transform of the original Q-space data as digitized from Ref. 44. As shown in Fig. 5(b), we are unable to reproduce the $G(r)$ function published in Ref. 44. Instead, our Fourier transform yields a $G(r)$ that is more in-line with the present measurements, with a peak at 1.60(2) Å, corresponding to the Si-O nearest neighbor distance, and a second peak at 1.96(2) Å corresponding to the fourfold coordinated Fe site. It is evident, by comparison with our $G(r)$ for liquid fayalite shown in Fig. 3, that the effect of truncating the $S(Q)$ at a lower $Q_{\max} = 16.94$ Å^{-1} is to broaden the real space peaks such that the Si-O and Fe-O nearest-neighbor peaks merge together. This explains why Waseda *et al.*[44] were unable to resolve both Fe-O distances observed in the present measurement and demonstrates the invaluable nature of synchrotron x-ray measurements with high-Q accessibility for resolving the local structure of liquids.

B. Structure of $(Fe_xCa_{1-x}O)_y(SiO_2)_{1-y}$ liquids and glasses

The two bond distances measured at $r_{\mathrm{FeO}} \approx 1.93$ and 2.2 Å unequivocally prove the presence of both FeO_4 and FeO_6 polyhedra in all of the $(Fe_xCa_{1-x}O)_y(SiO_2)_{1-y}$ compositions studied. The results for liquid fayalite ($x = 1, y = 0.667$) reveal an average coordination number of $\bar{n}^{\mathrm{O}}_{\mathrm{Fe}} = 4.8(2)$. It is difficult to assess to what extent this average coordination number arises from a mixture of FeO_4 and FeO_6, FeO_4, and FeO_5, or a coexistence of all three of these structural motifs. We would, however, expect the bond distance for fivefold coordinated Fe to be intermediate between that for the FeO_4 and FeO_6 polyhedra (2.06 Å for fivefold coordinated Fe^{2+}).[42] Since no peak is resolved at this intermediate position, it is unlikely that anymore than 5–10% fivefold coordinated Fe polyhedra exist within the liquid structure. If we therefore neglect the possible presence of FeO_5 species, then the coordination number can be described as a combination of FeO_4 and FeO_6 species using the expression $\bar{n}^{\mathrm{O}}_{\mathrm{Fe}} = 4\gamma + 6(1-\gamma)$, where γ is the fraction of FeO_4 species. This enables us to estimate the fraction of four and sixfold coordinated Fe species in liquid fayalite as up to 40(1)% FeO_6 and 60(1)% FeO_4. We see an increase in the concentration of FeO_6 polyhedra with reducing Fe content in the ferrosilite ($x = 1$, $y = 0.5$) liquid, which yields an average coordination number $\bar{n}^{\mathrm{O}}_{\mathrm{Fe}} = 5.1(2)$. This suggests the presence of up to 55(1)% FeO_6 and 45(1)% FeO_4 species. Due to the increasing complexity of pair correlations in the $G(r)$ for liquid hedenbergite ($x = 0.5$, $y = 0.5$), it is not possible to obtain a reliable Gaussian fit to the experimental data. It is, however, clear from the presence of a second Fe-O peak that a significant fraction of both four and sixfold coordinated Fe polyhedra are present in the liquid structure.

Extended x-ray absorption spectroscopy (EXAFS) measurements combined with simulation results for hedenbergite glass by Rossano *et al.*[23] indicate that iron occupies distorted fourfold and fivefold coordinated sites with oxygen. The present measurements do not entirely support this interpretation, since the sixfold Fe-O distance is clearly resolved in the $G(r)$ for glassy hedenbergite. Separate XAS measurements of $CaFeSiO_4$ and $Ca_{0.5}Fe_{0.5}SiO_3$ glasses also suggested that up to a third of the total Fe exhibits sixfold coordination.[14,19] It should be noted that, in the present diffraction measurements, a shift is observed in the position of the FeO_4 peak in the glass to $r_2 = 1.96(1)$ Å. This may be indicative of the presence of a small fraction of FeO_5 species. If we assume distances of 1.93 Å for fourfold and 2.06 Å for fivefold coordinated Fe, then the position 1.96 Å $= 0.77 \times 1.93 + 0.23 \times 2.06$ Å suggests the possible presence of 23% fivefold coordinated polyhedra,

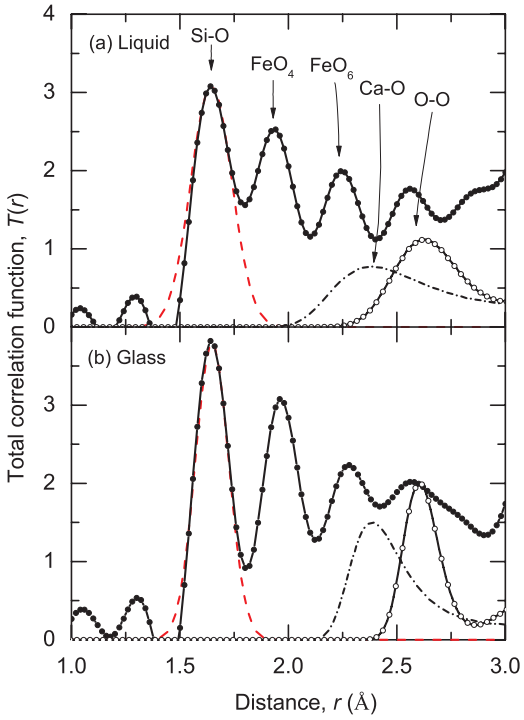

FIG. 6. (Color online) Measured $T(r)$ functions for (a) liquid, and (b) glassy hedenbergite. The black curves with solid circles represent the measured data, and the dashed (red) curves are Gaussian fits to the Si-O nearest-neighbor peak. The chained (black) curves and the black curves with open circles are the corresponding liquid and glassy $g_{CaO}(r)$ and $g_{OO}(r)$ partial pair distribution functions, respectively, as reported in Skinner *et al.*[64] and multiplied by their corresponding x-ray weighting factors for the $Fe_{0.5}Ca_{0.5}SiO_3$ composition. The positions of the Si-O, FeO_4, FeO_6, Ca-O, and O-O correlations are indicated by the arrows.

relative to the fraction of fourfold Fe species present. The interpretation of the hedenbergite composition is complicated by the additional Ca-O partial pair distribution function, which overlaps the Fe-O correlations. From previous measurements of calcium rich silicate and aluminate liquids and glasses, calcium tends to occupy a broad range of coordination sites, which leads to a very broad and often asymmetric pair distribution function.[43,49,64] This increases the level of ambiguity in the measured total pair distribution functions such that the individual partial pair correlations cannot be adequately modelled using a Gaussian fitting procedure. This is illustrated in Fig. 6. in which the $g_{CaO}(r)$ and $g_{OO}(r)$ partial pair distribution functions calculated by molecular dynamics computer simulations for both liquid and glassy $CaSiO_3$ from Ref. 64 are shown, after applying the appropriate x-ray weightings for the hedenbergite composition, together with the experimentally measured $T(r)$ functions for liquid and glassy hedenbergite. In order to obtain more detailed information on the fraction of Fe and Ca coordination species in the liquid and glassy hedenbergite structures, it would therefore be necessary to make more detailed measurements using, e.g., the method of neutron diffraction with isotope substitution and/or combine diffraction measurements with results from molecular dynamics computer simulations.

It is clear that our results do not confirm the previous interpretations of XAS measurements, which suggest a preponderance of four and fivefold coordinated Fe in iron silicate liquids and glasses of similar composition.[23,30,46,47] Our results instead support predictions from optical and Raman spectra that suggest a significant fraction of sixfold coordinated Fe^{2+} polyhedra.[6,17,18] Keppler[17] argued that the EXAFS evidence for Fe in tetrahedral coordination in silicate melts and glasses may be affected by positional disorder effects yielding significantly too short Fe-O distances and coordination numbers if the Fe cations occupy highly distorted octahedral sites. Indeed, Waychunas *et al.*[65] found that even in crystalline fayalite, erroneously short Fe-O distances and small coordination numbers are found using EXAFS due to the distorted octahedral M1 and M2 sites. Although anharmonic corrections to the data allow the determination of correct Fe-O bond distances in the crystal, small Fe-O bond distances and coordination numbers are still found in the glasses and melts. In addition to EXAFS, the x-ray absorption near edge structure (XANES) technique has also been commonly employed to determine the local coordination environment of Fe in silicate melts and glasses.[22,34,36] In this technique, the pre-edge intensity can indicate a change in coordination geometry. However, in order to interpret this accurately, the result must be combined with knowledge from the first maximum of the EXAFS oscillation, which is inversely proportional to the Fe-O bond distance.[34] The EXAFS measurements only yield the average bond distance and as such may arise from a combination of various coordination sites. In fact the bond distance $r_{FeO} = 1.98(2)$ measured for liquid fayalite by Jackson *et al.*[46] using EXAFS, and corrected for anharmonic effects, lies within 3% of the average bond length calculated for liquid fayalite from the present diffraction measurements, where $\bar{r}_{FeO} = 1.93\gamma + 2.20(1-\gamma) = 2.04(2)$ Å is obtained using $\gamma = 0.4$, i.e., the fraction of FeO_4 species determined from the Gaussian fit of the liquid $G(r)$. The average bond distances and coordination numbers obtained from spectroscopic and diffraction measurements of various ferrosilicate liquids and glasses are given in Table II. The present diffraction results yield similar average Fe-O bond distances as in many of the previous XAS studies (within a few percent). It is evident that the XAS measurements could be interpreted by a wider distribution of Fe coordination sites and caution should therefore be used when inferring the Fe coordination number from XAS measurements of iron silicate liquids and glasses in order to account for the significant fractions of sixfold coordinated Fe revealed in the present study.

C. Structure of liquid and glassy basalt

The measured $G(r)$ function in the low-r region for liquid basalt is shown in Fig. 7. For comparison, the $g_{\alpha\beta}(r)$ partials for liquid Anorthite-Diopside $(CaAl_2Si_2O_8)_{0.36}(CaMgSi_2O_6)_{0.64}$ (denoted $An_{36}Di_{64}$), as calculated by Vuilleumier *et al.*[66] using *ab initio* molecular dynamics computer simulations, are also shown. The $An_{36}Di_{64}$ is a common model basaltic compound and the simulations represent the closest comparison to our diffraction measurements that is available in the literature. The $g_{\alpha\beta}(r)$ functions have been multiplied by their appropriate x-ray weightings for the basalt composition. The first peak in

TABLE II. Reported Fe-O bond distances r_{FeO} and coordination numbers $\bar{n}^{O}_{Fe}$ for various ferrosilicate liquids and glasses, of similar composition to the samples studied in the present work, as measured using EXAFS and XANES techniques. The results of the present x-ray diffraction (XRD) measurements for liquid fayalite and ferrosilite are also given, where the average Fe-O distances were obtained using the expression $\bar{r}_{FeO} = 1.93\gamma + 2.20(1-\gamma)$, where 1.93 and 2.20 (Å) are the measured Fe-O bond distances for four- and sixfold coordinated Fe, respectively, and γ is the fraction of fourfold coordinated Fe species determined from the Gaussian fitting procedure [see Fig. 4].

Sample	State	r_{FeO} (Å)	$\bar{n}^{O}_{Fe}$	Technique	Ref.
Fe_2SiO_4	Liquid	1.98(2)	4	EXAFS	46
Fe_2SiO_4	Liquid	2.04(2)	4.8(2)	XRD	Present work
$FeSiO_3$	Liquid	2.08(2)	5.1(2)	XRD	Present work
$CaFeSiO_4$	Glass	1.91	4.7	XAFS	19
$Ca_{0.5}Fe_{0.5}SiO_3$	Glass	1.92	4.5	XAFS	19
$Ca_{0.5}Fe_{0.5}SiO_3$	Glass	1.99(1)	3.9(3)	EXAFS	23
$Li_2FeSi_3O_8$	Glass	2.03(2)	4.7(2)	EXAFS	30
$Rb_2FeSi_3O_8$	Glass	2.00(2)	4.3(2)	EXAFS	30
$Na_2FeSi_3O_8$	Glass	2.02(2), 2.06[a]	4, 4-5[a]	EXAFS, XANES	47
$K_2FeSi_3O_8$	Glass	2.00(2), 2.04[a]	4, 4-5[a]	EXAFS, XANES	47

[a]Indicates values corrected for anharmonicity by Jackson *et al.*[30]

the $G(r)$ for liquid basalt at 1.66(1) Å is consistent with the position of the nearest neighbor Si-O correlations found in the $An_{36}Di_{64}$ liquid simulations. If we attribute the peak measured at 2.72(3) Å for the liquid and 2.69(3) Å for the glassy basalt to O-O correlations, then the ratios $r_{OO}/r_{SiO} = 1.639$ and 1.630 in the liquid and glass, respectively, are both very close to the ideal tetrahedral ratio of $\sqrt{(8/3)} = 1.633$.

The $An_{36}Di_{64}$ composition does not contain any iron. The peaks observed at 1.84 and 2.25 Å in the measured basalt $G(r)$ at similar distances to the Fe-O distances observed in the previous iron silicate compositions, and their absence in the re-weighted $An_{36}Di_{64}$ partials, points to the presence of fourfold and sixfold coordinated Fe species in both the liquid and glassy basalt. The variation in Fe-O distance from the values of $r_{FeO} = 1.93$ and 2.20 Å measured in the simpler iron silicate compositions arises from the overlap by other

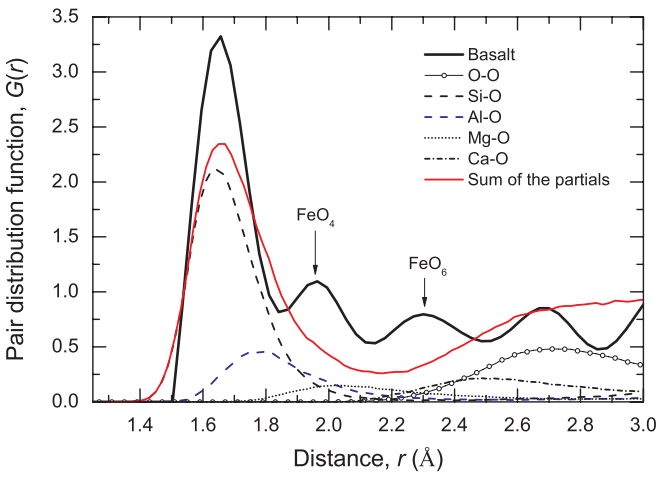

FIG. 7. (Color online) The $G(r)$ function for liquid basalt shown together with the partials calculated from *ab initio* molecular dynamics computer simulations of an An-Di liquid[66] and multiplied by their respective x-ray weighting factors in the basalt composition used in this study. The positions of the FeO_4 and FeO_6 peaks are indicated by the arrows. For clarity, only the correlations involving oxygen are shown.

pair distribution functions in this significantly more complex multicomponent system.

The confirmation of sixfold coordinated iron in the natural basaltic, olivine and pyroxene melts measured in this study has important implications for the modeling and understanding of magmatic and volcanic processes. The present diffraction results show that Fe ions occupy fewer octahedral sites in the melt than in the corresponding crystal and the ratio of four- to sixfold coordinated Fe sites may effect, e.g., the partitioning behavior of these ions.[42] The viscosity of melts also governs the production, transport and eruption of magmas.[67,68] In general, it is believed that fourfold Fe acts as a network former in silicate melts, whereas sixfold coordinated Fe will act as a network modifier.[42] The proportion of four to sixfold coordinated Fe ions therefore has significant influence on the viscosity of magmatic melts, where the greater the proportion of fourfold Fe, the higher the viscosity will be. This influences the high pressure behavior of magmatic liquids as the pressure dependency of viscosity is related to the proportion of fourfold coordinated Fe present at ambient pressure. The present ambient pressure study, therefore, provides an important benchmark for interpreting the structural and physicochemical changes that occur in iron silicate liquids at high pressure.[50]

VII. CONCLUSIONS

We have reported high-quality *in situ* synchrotron x-ray diffraction measurements of (Fe,Ca)O-SiO_2 liquids together with a basalt composition. The results reveal direct evidence of a coexistence of both four and sixfold coordinated Fe species in all compositions measured with up to 40(1)% and 55(1)% sixfold coordinated Fe octahedra observed in the fayalite and ferrosilite liquids, respectively. Previous diffraction measurements on molten iron silicates were unable to resolve the sixfold coordination environment due in part to poor real-space resolution associated with the limited Q-space accessibility of conventional x-ray diffractometers. Previous XAS studies have suggested a preponderance of fourfold coordinated Fe species present in liquid fayalite. We show that this discrepancy can be reconciled by consulting the average Fe-O bond distance

obtained from both diffraction and XAS techniques. These average Fe-O distances are comparable and since the diffraction results reveal unequivocal evidence for significant fractions of sixfold coordinated Fe, the XAS results must be representative of a wider distribution of Fe coordination sites than previously reported. The presence of both fourfold and sixfold coordinated Fe was also confirmed in the $G(r)$ measured for a liquid and glassy basalt composition and the results have important consequences for the partitioning behavior of Fe ions and the production and transport of magmas as the coordination environment in the liquid under ambient conditions influences the pressure dependence of viscosity in magmatic melts.

ACKNOWLEDGMENTS

We thank Gaëlle Prouteau for providing us with the basalt sample. We also thank Jérome Andrieux and the staff at the ID15 beamline, ESRF. Chris Hayward and Holly Spice are gratefully acknowledged for their contributions to the electron probe microanalysis and we thank Bertrand Guillot for providing the MD partials for $An_{36}Di_{64}$ from Ref. 66 and Lawrie Skinner for providing the MD partials for $CaSiO_3$ from Ref. 64. This work was supported by the European Research Council under the European Community's Seventh Framework Programme (FP7/20072013 grant agreement No. 259649 to C.S.).

*james.drewitt@ed.ac.uk

[1]M. Wilke, Ann. Geophys. **48**, 609 (2005).
[2]A. Kondratiev and E. Jak, Metall. Mater. Trans. B **32**, 1015 (2001).
[3]K. Hanke, Beitr. Mineral. Petrol. **11**, 535 (1965).
[4]S. Sueno, M. Cameron, and C. T. Prewitt, Am. Mineral. **61**, 38 (1976).
[5]M. Cameron, S. Sueno, C. T. Prewitt, and J. J. Papike, Am. Mineral. **58**, 594 (1973).
[6]J. A. Boon and W. S. Fyfe, Chem. Geol. **10**, 287 (1972).
[7]P. M. Bell and H. K. Mao, Carnegie Instn. Wash. Year Book **73**, 496 (1974).
[8]E. Takahashi, Geochim. Cosmochim. Acta **42**, 1829 (1978).
[9]D. A. Nolet, R. G. Burns, S. L. Flamm, and J. R. Besancon, in *Proceedings 10th Lunar and Planetary Science Conference, Houston, Tex, 19-23 March 1979*, Vol. 2 (Pergamon Press, New York, 1979), pp. 1775–1786.
[10]D. S. Goldman and J. I. Berg, J. Non-Cryst. Solids **38-39**, 183 (1980).
[11]G. Calas and J. Petiau, Solid State Commun. **48**, 625 (1983).
[12]B. O. Mysen, D. Virgo, E. R. Neumann, and F. Seifert, Am. Mineral. **70**, 317 (1985).
[13]D. Virgo and B. O. Mysen, Phys. Chem. Miner. **12**, 65 (1985).
[14]N. Binsted, G. N. Greaves, and C. M. B. Henderson, J. Phys. (Colloques) **47**, C8-837 (1986).
[15]N. Iwamoto, N. Umesaki, and T. Atsumi, J. Mater. Sci. Lett. **6**, 271 (1987).
[16]B. Hannoyer, M. Lenglet, J. Dürr, and R. Cortes, J. Non-Cryst. Solids **151**, 209 (1992).
[17]H. Keppler, Am. Mineral. **77**, 62 (1992).
[18]Z. Wang, T. F. Cooney, and S. K. Sharma, Contrib. Mineral. Petrol. **115**, 112 (1993).
[19]C. M. B. Henderson, G. Cressey, and S. A. T. Redfern, Radiat. Phys. Chem. **45**, 459 (1995).
[20]H. V. Alberto, J. L. Pinto da Cunha, B. O. Mysen, J. M. Gil, and N. Ayres de Campos, J. Non-Cryst. Solids **194**, 48 (1996).
[21]S. Rossano, E. Balan, G. Morin, J. P. Bauer, G. Calas, and C. Brouder, Phys. Chem. Miner. **26**, 530 (1999).
[22]Z. Wu, M. Bonnin-Mosbah, J. P. Duraud, N. Métrich, and J. S. Delaney, J. Synchrotron. Rad. **6**, 344 (1999).
[23]S. Rossano, A. Ramos, J. M. Delaye, S. Creux, A. Filipponi, C. Brouder, and G. Calas, Europhys. Lett. **49**, 597 (2000).
[24]J. M. Burkhard, J. Non-Cryst. Solids **275**, 175 (2000).
[25]L. Galoisy, G. Calas, and M. A. Arrio, Chem. Geol. **174**, 307 (2001).
[26]G. Giuli, G. Pratesi, C. Cipriani, and E. Paris, Geochim. Cosmochim. Acta. **66**, 4347 (2002).
[27]G. Giuli, E. Paris, G. Pratesi, C. Koeberl, and C. Cipriani, Meteorit. Planet. Sci. **38**, 1181 (2003).
[28]N. Zotov, J. Non-Cryst. Solids **323**, 1 (2003).
[29]F. Farges, Y. Lefrére, S. Rossano, A. Berthereau, G. Calas, and G. E. Brown, J. Non-Cryst. Solids **344**, 176 (2004).
[30]W. E. Jackson *et al.*, Geochim. Cosmochim. Acta **69**, 4315 (2005).
[31]B. O. Mysen, Geochim. Cosmochim. Acta **70**, 2337 (2006).
[32]C. Weigel, L. Cormier, L. Galoisy, G. Calas, D. Bowron, and B. Beuneu, Appl. Phys. Lett. **89**, 141911 (2006).
[33]M. Wilke, C. Schmidt, F. Farges, V. Malavergne, L. Gautron, A. Simionovici, M. Hahn, and P.-E. Petit, Chem. Geol. **229**, 144 (2006).
[34]M. Wilke, F. Farges, G. M. Partzsch, C. Schmidt, and H. Behrens, Am. Mineral. **92**, 44 (2007).
[35]S. Rossano, H. Behrens, and M. Wilke, Phys. Chem. Miner. **35**, 77 (2008).
[36]G. Giuli, S. G. Eeckhout, C. Koeberl, G. Pratesi, and E. Paris, Meteorit. Planet. Sci. **43**, 981 (2008).
[37]B. Cochain, D. R. Neuville, D. de Ligny, J. Roux, F. Bauselet, E. Strukelj, and P. Richet, J. Phys.: Conf. Series **190**, 012182 (2009).
[38]E. Cottrell, K. A. Kelley, A. Lanzirotti, and R. A. Fischer, Chem. Geol. **268**, 167 (2009).
[39]A. Di Muro, N. Métrich, M. Mercier, D. Giordano, D. Massare, and G. Montagnac, Chem. Geol. **259**, 78 (2009).
[40]B. Cochain, D. R. Neuville, G. S. Henderson, C. A. McCammon, O. Pinet, and P. Richet, J. Am. Ceram. Soc. **95**, 962 (2012).
[41]G. Giuli, R. A. Mori, M. R. Cicconi, E. Paris, P. Glatzel, S. G. Eeckhout, and B. Scaillet, Am. Mineral. **97**, 468 (2012).
[42]G. E. Brown, F. Farges, and G. Calas, in *Rev. Mineral.*, Vol. 32, edited by J. F. Stebbins, P. McMillan, and D. B. Dingwell (The Mineralogical Society of America, Wahington, USA, 1995) pp. 317–410.
[43]J. W. E. Drewitt, L. Hennet, A. Zeidler, S. Jahn, P. S. Salmon, D. R. Neuville, and H. E. Fischer, Phys. Rev. Lett. **109**, 235501 (2012).
[44]Y. Waseda and J. M. Toguri, Metall. Trans. B **9**, 595 (1978).
[45]Y. Waseda, Y. Shiraishi, and J. M. Toguri, Trans. JIM **21**, 51 (1980).
[46]W. E. Jackson, J. Mustre de Leon, G. E. Brown, Jr., G. A. Waychunas, S. D. Conradson, and J. M. Combes, Science **262**, 229 (1993).

[47]G. A. Waychunas, G. E. Brown, C. W. Ponader, and W. E. Jackson, Nature (London) **350**, 251 (1988).
[48]L. Hennet, V. Cristiglio, J. Kozaily, I. Pozdnyakova, H. E. Fischer, A. Bytchkov, J. W. E. Drewitt, M. Leydier, D. Thiaudière, S. Gruner, S. Brassamin, D. Zanghi, G. J. Cuello, M. Koza, S. Magazù, G. N. Greaves, and D. L. Price, Eur. Phys. J. Special Topics **196**, 151 (2011).
[49]J. W. E. Drewitt, S. Jahn, V. Cristiglio, A. Bytchkov, M. Leydier, S. Brassamin, H. E. Fischer, and L. Hennet, J. Phys.: Condens. Matter **23**, 155101 (2011); **24**, 099501 (2012).
[50]C. Sanloup, J. W. E. Drewitt, C. Crépisson, Y. Kono, C. Park, C. McCammon, L. Hennet, S. Brassamin, and A. Bytchkov, Geochim. Cosmochim. Acta (2013), 10.1016/j.gca.2013.05.012.
[51]T. E. Faber and J. M. Ziman, Philos. Mag. **11**, 153 (1965).
[52]A. Zeidler, J. W. E. Drewitt, P. S. Salmon, A. C. Barnes, W. A. Crichton, S. Klotz, H. E. Fischer, C. J. Benmore, S. Ramos, and A. C. Hannon, J. Phys.: Condens. Matter **21**, 474217 (2009).
[53]B. E. Warren, H. Krutter, and O. Morningstar, J. Am. Ceram. Soc. **75**, 202 (1936).
[54]I. Di Carlo, M. Pichavant, S. G. Rotolo, and B. Scaillet, J. Petrol. **47**, 1317 (2006).
[55]M. Pichavant, I. Di Carlo, Y. Le Gac, S. G. Rotolo, and B. Scaillet, J. Petrol. **50**, 601 (2009).
[56]L. Cemič and E. Dachs, Phys. Chem. Miner. **33**, 457 (2006).
[57]A. Bytchkov, L. Hennet, I. Pozdnyakova, J. Wright, G. Vaughan, S. Rossano, K. Madjer, and D. L. Price, AIP Conf. Proc. **1234**, 219 (2010).
[58]A. P. Hammersley, FIT2D*V9.129 Reference Manual V3.1*, ESRF98HA01T (ESRF Internal Report, 1998).
[59]A. P. Hammersley, S. O. Svensson, M. Hanfland, A. N. Fitch, and D. Häusermann, High Pressure Res. **14**, 235 (1996).
[60]J. H. Hubbell, W. J. Veigele, E. A. Briggs, R. T. Brown, D. T. Cromer, and R. J. Howerron, J. Phys. Chem. Ref. Data **4**, 471 (1975).
[61]E. N. Maslen, A. G. Fox, and M. A. O'Keefe, *International Tables for X-ray Crystallography*, edited by A. J. C. Wilson, Vol. C (Dordrecht, Kluwer, 1995), p. 476.
[62]Y. Shiraishi, K. Ikeda, A. Tamura, and T. Saitô, Trans. Jpn. I. Met. **19**, 264 (1978).
[63]C. Hayward, Holocene **22**, 119 (2011).
[64]L. B. Skinner, C. J. Benmore, S. Tumber, L. Lazareva, J. Neuefeind, L. Santodonato, J. Du, and J. B. Parise, J. Phys. Chem. B **116**, 13439 (2012).
[65]G. A. Waychunas, G. E. Brown, and M. J. Apted, Phys. Chem. Miner. **13**, 31 (1986).
[66]R. Vuilleumier, N. Sator, and B. Guillot, Geochim. Cosmochim. Acta **73**, 6313 (2009).
[67]D. B. Dingwell, Elements **2**, 281 (2006).
[68]P. Papale, Nature (London) **397**, 425 (1999).